Supporting Information

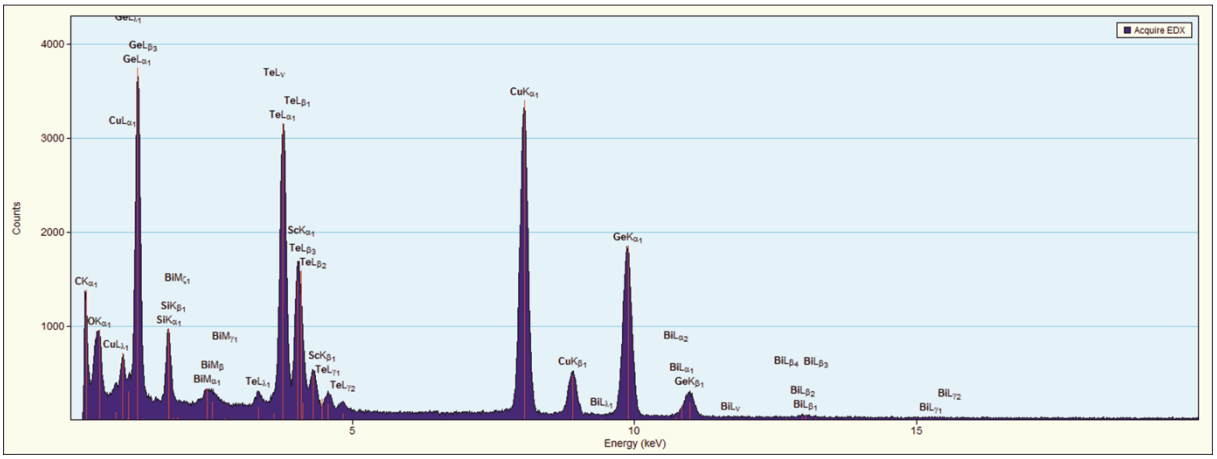

Figure S1. A representative EDX spectra for 0.962(GeTe) 0.038($Bi_2Se_{0.2}Te_{2.8}$) (the sample with the lowest Bi content). As also stated in the manuscript the Bi M-line is observed.

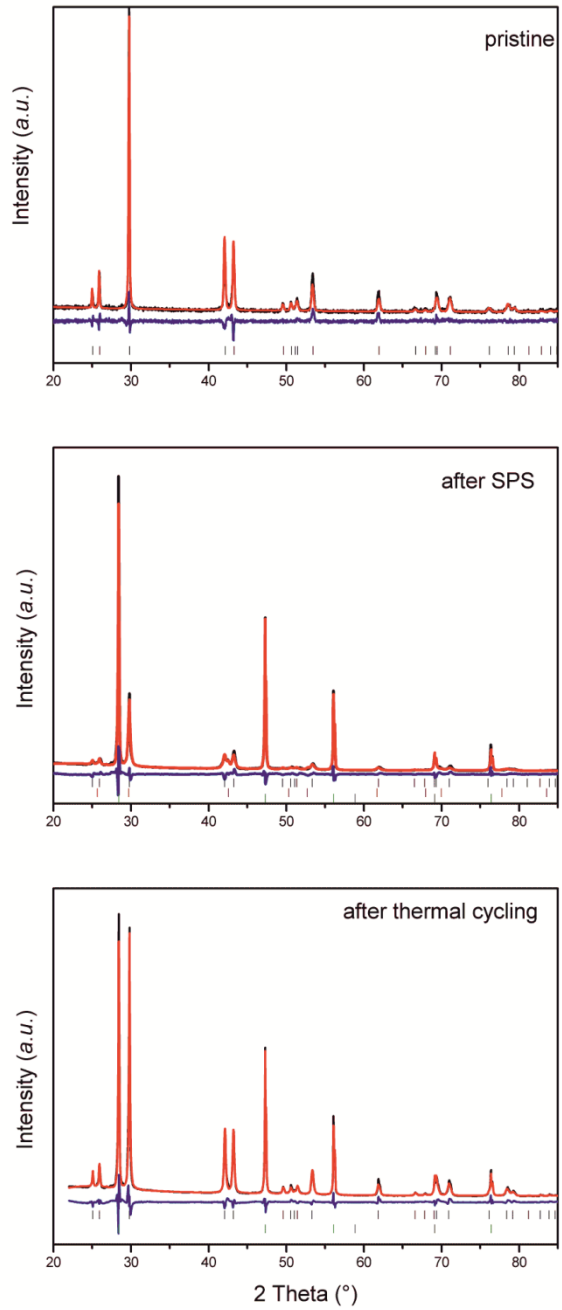

Figure S2. Fitted XRD pattern of $(GeTe)_{0.937}(Bi_2Te_{2.8}Se_{0.2})_{0.063}$ at 28 °C in the pristine stage, after SPS and after thermal cycling. Observed (black), calculated (red) and difference curves (blue) are shown, reflection positions indicated by vertical bars.

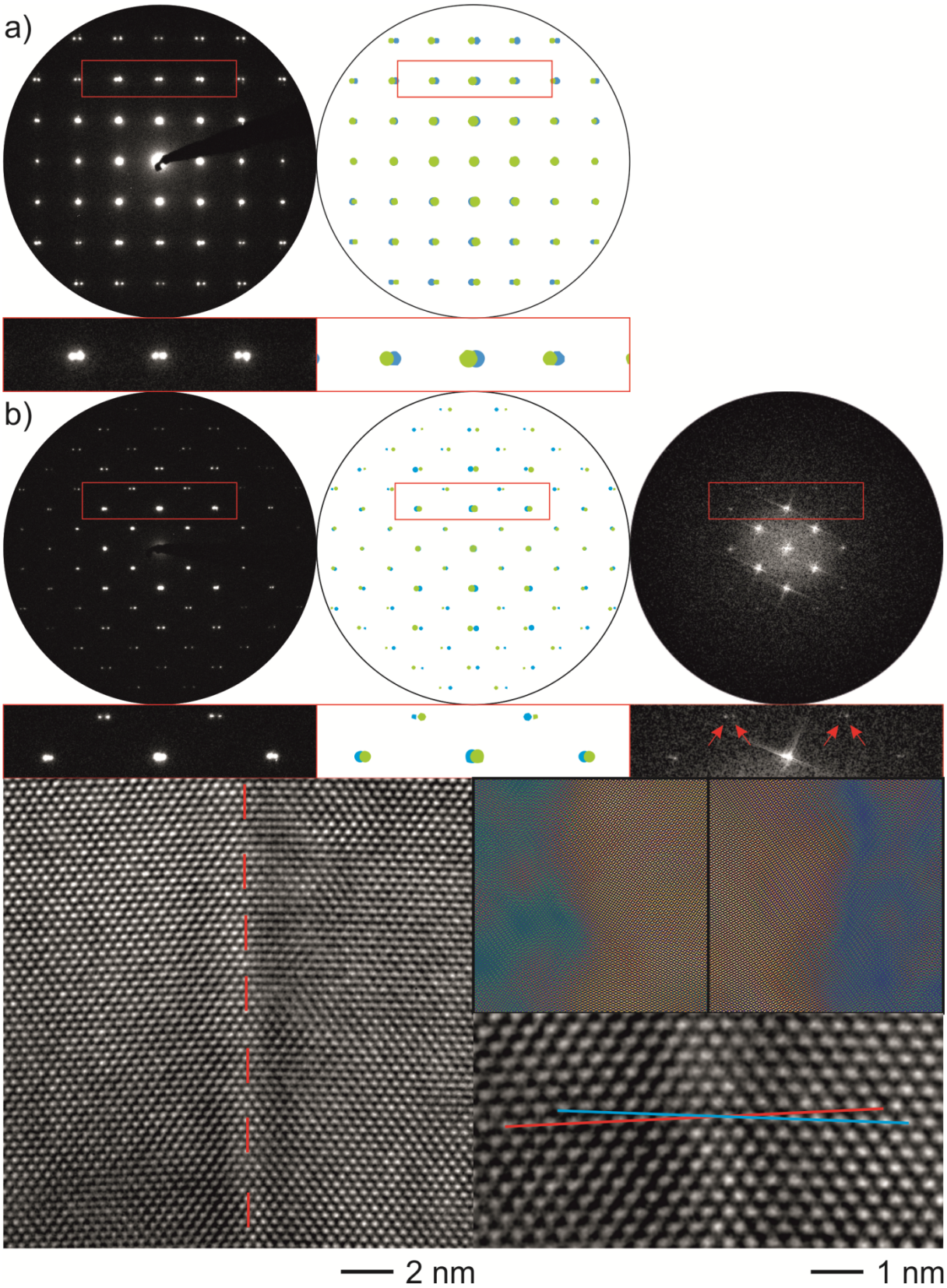

Figure S3. Figure a depicts a precession electron diffraction (PED) along [1-11] zone axis with a twin boundary along (110). The right image represents the respective superimposed calculated diffraction patterns for the different twin domains. Figure b depicts a PED, superimposed calculated diffraction pattern, FFT and HRTEM along [-110] with a twin boundary along (112). The HRTEM micrograph depicts an on edge twin boundary (marked with a red dashed line). The right images represent the inverse fourier filtering of the different

twin domains. The image below shows an enlarged section of the twin boundary with the red and the blue lines guiding the eye along the two twin domains.

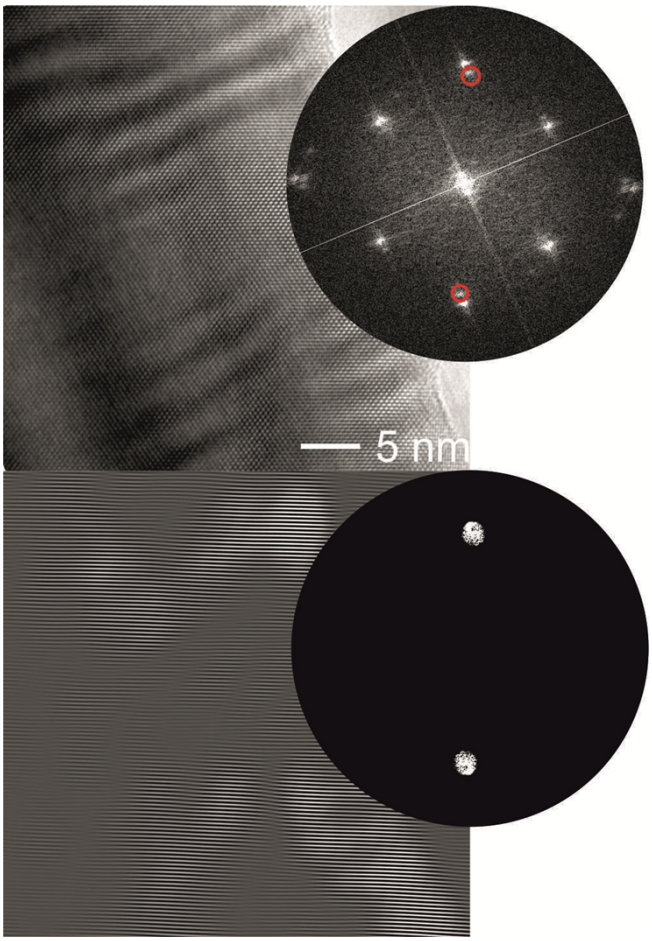

Figure S4. IFFT filtering of fringes in $(GeTe)_{0.937}(Bi_2Se_{0.2}Te_{2.8})_{0.063}$. The top and the bottom images depict the HRTEM micrograph and the IFFT filtered image, respectively. The red circle in the FFT marks the diffraction spot used for IFFT filtering.

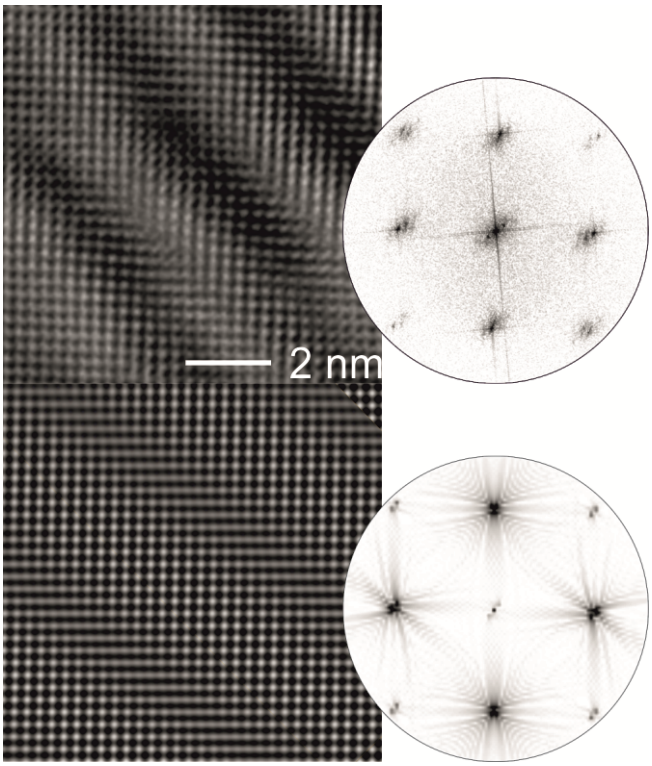

Figure S5. The top image represents a HRTEM micrograph and FFT of the observed fringes in <-110> zone axis. The image below represents the superposition of calculated HRTEM micrographs of α and β phase and the corresponding FFT.

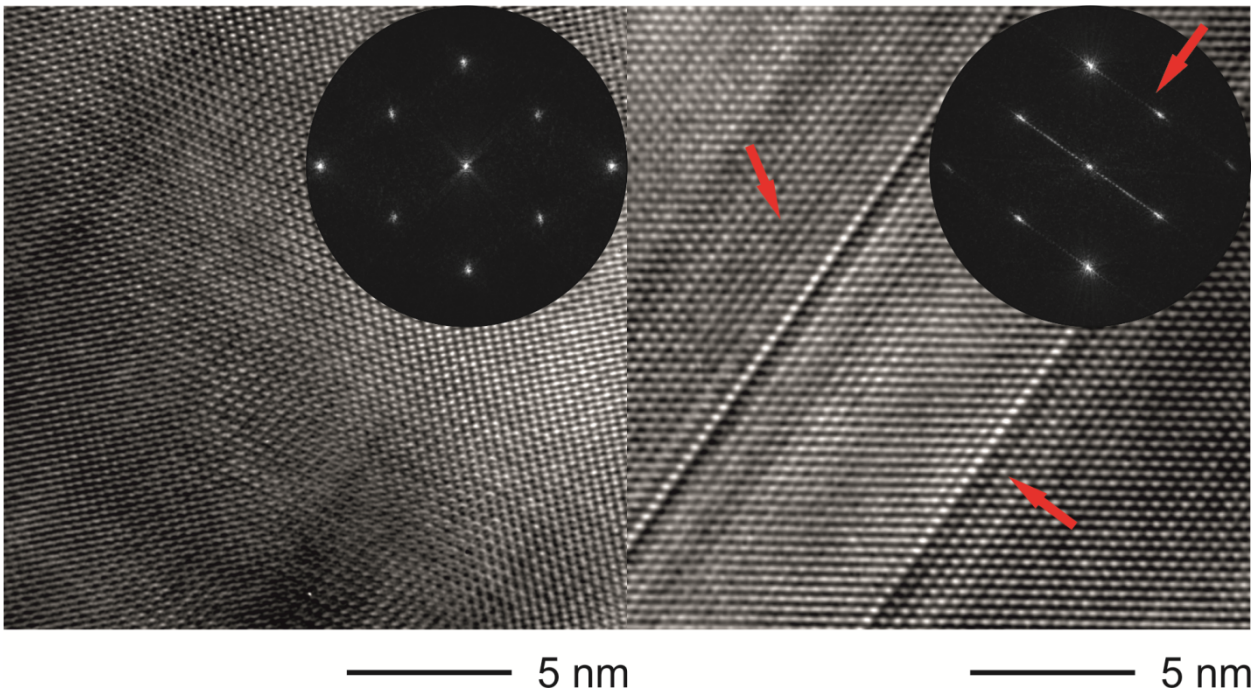

Figure S6: Comparison of representative regions of the samples in state 3 for $(GeTe)_{0.962}(Bi_2Se_{0.2}Te_{2.8})_{0.038}$ (left) and $(GeTe)_{0.937}(Bi_2Se_{0.2}Te_{2.8})_{0.063}$ (right). For sample $(GeTe)_{0.937}(Bi_2Se_{0.2}Te_{2.8})_{0.063}$ formation of planar defects along <111> and <001> directions are observed which are absent in the sample $(GeTe)_{0.962}(Bi_2Se_{0.2}Te_{2.8})_{0.038}$ (right). The insets show FFTs of the corresponding areas. In the case of $(GeTe)_{0.937}(Bi_2Se_{0.2}Te_{2.8})_{0.063}$ diffuse intensities correlate to the planar defects (marked with red arrows).

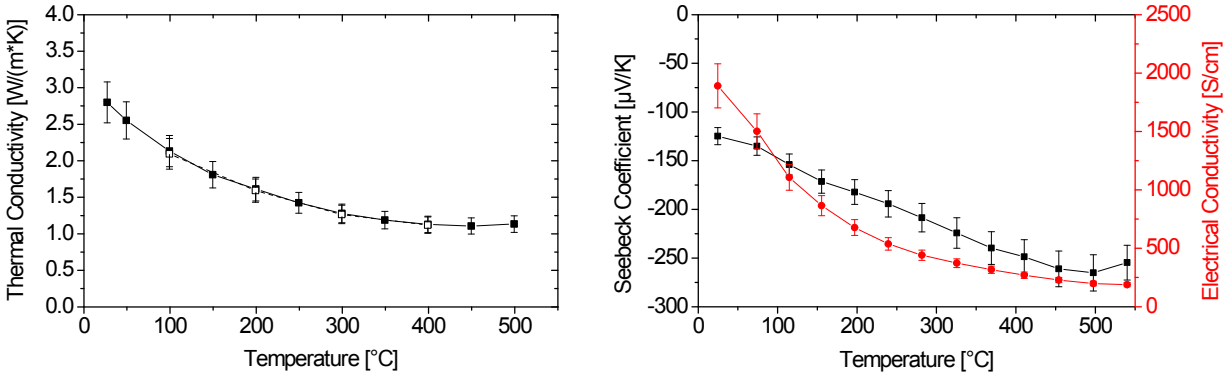

Figure S7. Transport data of SPS-compacted Bi-doped PbTe in dependence on temperature. Left: Thermal conductivity. Right: Seebeck coefficient (black) and electrical conductivity (red). Full data points: heating, empty points: cooling

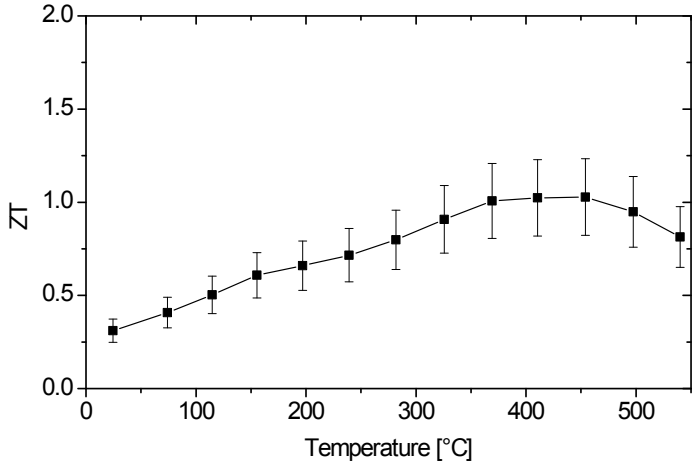

Figure S8. Figure of merit ZT of SPS-compacted Bi-doped PbTe in dependence on temperature. For calculating the ZT value for the highest temperature, the thermal conductivity value was extrapolated from the data obtained up to 500°C.

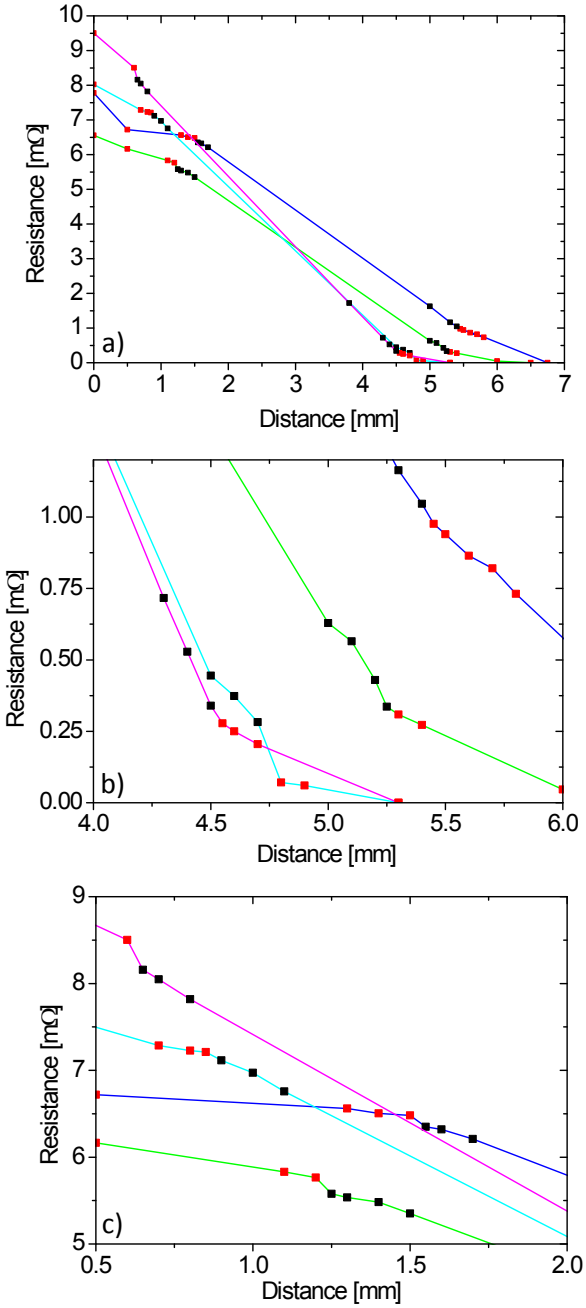

Figure S9. Plot of resistance versus distance between probing needle and front contact for different material / contact combinations. Black points = $(GeTe)_{1-x}(Bi_2Se_{0.2}Te_{2.8})_x$ (thermoelectric material), red points = SnTe (contact). Near the leg/contact interface, the number of acquired data points was significantly increased in order to accurately determine the voltage drop corresponding to contact resistance. a) Resistance / distance plot for whole leg + contacts, b) leg + front contact, c) leg + back contact, both magnified sections from plot a.

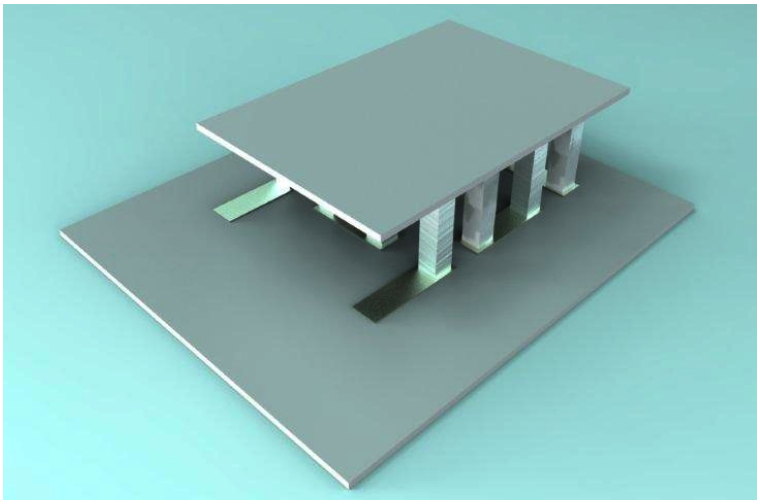

Figure S10. Drawing of assembled thermoelectric module.